Achieving the Heisenberg limit with Dicke states in noisy quantum metrology

Zain H. Saleem,[1,*] Michael Perlin,[2,†] Anil Shaji,[3,‡] and Stephen K. Gray[4,§]

[1]*Mathematics and Computer Science Division, Argonne National Laboratory, 9700 S Cass Ave, Lemont, Illinois 60439, USA*

[2]*Infleqtion, Inc., Chicago, Illinois 60615, USA*

[3]*School of Physics, IISER Thiruvananthapuram, Kerala, India 695551*

[4]*Center for Nanoscale Materials, Argonne National Laboratory, Lemont, Illinois 60439, USA*

(Received 16 October 2023; revised 1 March 2024; accepted 22 April 2024; published 9 May 2024)

Going beyond the standard quantum limit in noisy quantum metrology is an important and challenging task. Here we show how Dicke states can be used to surpass the standard quantum limit and achieve the Heisenberg limit in open quantum systems. The system we study has qubits symmetrically coupled to a resonator, and our objective is to estimate the coupling between the qubits and the resonator. The time-dependent quantum Fisher information with respect to the coupling is studied for this open quantum system where the same decay rates are assumed on all qubits. We show that when the system is initialized to a Dicke state with an optimal excitation number one can go beyond the standard quantum limit and achieve the Heisenberg limit even for finite values of the decays on the qubit and the resonator, particularly when the qubits and resonator are strongly coupled. We compare our results against the highly entangled GHZ state and a completely separable state and show that the GHZ state performs quite poorly, whereas under certain noise conditions the separable state is able to go beyond the standard quantum limit due to subsequent interactions with a resonator.

DOI: 10.1103/PhysRevA.109.052615

I. INTRODUCTION

A quantum probe with N elementary subunits is the focus of discussions on quantum-limited single parameter estimation [1–4]. The probe is chosen such that the parameter to be estimated appears in its Hamiltonian. A suitable initial state of the probe evolves for a fixed time in a manner that depends on the parameter value. The value can be then inferred from a read-out of the final state of the probe. Quantum mechanics places a fundamental limit on measurement precision, called the Heisenberg limit (HL), which constrains how the precision of parameter estimation improves as the number of probe units increases. According to the HL, scaling of the precision with the number of elementary subunits cannot scale better than $1/N$. For a noiseless system, HL scaling can be saturated using entangled states of the probe [5]. In practice, though, environmental decoherence typically degrades metrologically useful entanglement; instead of HL, precision scales like $1/\sqrt{N}$, called the standard quantum limit (SQL), which can be achieved by using the N elementary subunits independently. The burgeoning area of noisy quantum metrology seeks to characterize and mitigate the detrimental effects of noise [6–23]. For example, to surpass the SQL various clever strategies have been devised, such as squeezing the vacuum [6], monitoring the environment during the measurements [7], quantum error correction [8–14], the use of graph states [15], and taking advantage of non-Markovian dynamics [16–18] of the probe.

The quantum Cramér-Rao bound [24] dictates that the precision in the measurement of a parameter in a quantum experiment is bounded by the inverse of the quantum Fisher information (QFI). The QFI is a time-dependent quantity which, in open quantum systems, first grows as the target signal gets imprinted into the system, before decreasing as decoherence randomizes the system and degrades the signature of the target signal. The best precision in the estimate of a parameter can, in such cases, be achieved by performing measurements near the times when the QFI is the largest [22,23].

In this paper, we introduce a strategy for surpassing the SQL in a noisy quantum system by making use of an optimal measurement time. We numerically explore the advantages of using the optimum measurement time when the quantum probe is initialized in Dicke states [25,26] with appropriately chosen excitation numbers. We also compare the measurement precision and its scaling obtained using Dicke states with that of highly entangled states like the GHZ state on one hand and simple X-polarized product states on the other, and find that in certain noise regimes, when optimizing over measurement time, even the product state can yield better than SQL scaling.

We investigate a qubit-cavity model in contact with an environment where both the qubits and the cavity are allowed to decay under the influence of noise from the environment. The parameter that is estimated is the coupling constant of the qubits to the cavity. The qubits constitute the quantum probe, and we focus on studying the scaling of the uncertainty in its estimate with the number of qubits, N. We calculate the

*zsaleem@anl.gov
†mika.perlin@gmail.com
‡shaji@iisertvm.ac.in
§gray@anl.gov

scaling of the time-optimized QFI with N and see for what choices of the initial states and decay rates of the qubits and the resonator we are able to surpass the SQL. The Hamiltonian of our system is permutationally symmetric, and this symmetry allows us to use a basis that reduces the dimensions of our problem and thus allows us simulate open quantum systems with relatively large values of N that would otherwise be computationally intractable. Dicke states are examples of permutationally symmetric states, and we will show that when the excitation number of the Dicke states is chosen appropriately and the measurements are performed in an optimal time region, we can surpass the standard quantum limit even in the presence of dissipation.

It is important to note that there are "no-go" theorems and also particular scenarios for which it has been established that open systems described by the Lindblad master equation cannot exhibit scaling beyond the standard quantum limit. In particular, Refs. [8,9] establish for systems such as we explore that an upper limit on the QFI scales linearly with the total probing time in a sequential scheme, which implies that the best one could hope to achieve is the SQL. If one were to assume that the corresponding total probing time in the parallel, N-qubit case is proportionate to N times some *fixed* (smaller) probing time, then one would also expect no better than SQL scaling with N. Our focus, however, is the case where measurements are performed at optimal times when the QFI is maximum, and these times vary with N. That these probing times are not fixed with N allows us to circumvent the no-go theorems. Of course, a negative aspect of our approach is that it is more complicated than schemes with fixed probing times, but we have suggested an experimental protocol that can offer some efficiencies [23].

The significance of our results and our main motivation lies in the fact that Dicke states with modest excitation numbers can be realized in the laboratory [27–37] and exploring the interplay between noise and metrological precision can be investigated experimentally. Indeed, there are a few proposals for using Dicke states and closely related states in specific quantum metrology schemes, including noisy quantum metrology as well [21,22,38,39]. See also the review articles Refs. [40] and [4] for additional discussion of Dicke states in quantum metrology. In addition there are multiple theoretical proposals for producing such states in the laboratory [41–52], giving further relevance to our work.

A. Quantum Fisher information

Consider the problem of estimating a (scalar) parameter θ in a quantum experiment and denote the (unbiased) estimator of this parameter by $\hat{\theta}$. The parameter-dependent evolution of the probe is given by $H_{\text{probe}} = \theta h$, where h is an operator on the probe state. The variance in the estimate of the parameter, $\delta\hat{\theta}^2$, is upper bounded by the quantum Cramér-Rao bound [53],

$$\delta\hat{\theta}^2 \geqslant \frac{1}{MF(\theta)}, \tag{1}$$

where M stands for the total number of application of the quantum probe and $F(\theta)$ is the QFI, which quantifies the responsiveness of the quantum state of the probe to changes in the measured parameter θ. The QFI of a mixed state $\rho = \sum_a \lambda_a |\lambda_a\rangle\langle\lambda_a|$ with respect to the parameter θ is [54]

$$F(\theta) = 2\sum_{a,b} \frac{|\langle\lambda_a|\partial_\theta \rho|\lambda_b\rangle|^2}{\lambda_a + \lambda_b}, \tag{2}$$

where the sum is taken over values of a, b for which $\lambda_a + \lambda_b \neq 0$. For closed evolution of the probe, the QFI has a quadratic time dependence, while for open evolution an optimal measurement time may be present that the parameter estimation protocol would take advantage of [23]. We study the scaling of the peak value of QFI under open evolution as N gets larger.

II. MODEL SYSTEM

The qubit-cavity model that we study here is described by the Hamiltonian ($\hbar = 1$)

$$H = \omega_q S_z + \omega_c a^\dagger a + g(a^\dagger S_- + a S_+), \tag{3}$$

where $S_z = \frac{1}{2}\sum_{j=1}^N \sigma_z^{(j)}$, and $S_\pm = \sum_{j=1}^N \sigma_\pm^{(j)}$ are collective spin operators expressed in terms of the single-qubit Pauli matrices $\sigma_z = |\uparrow\rangle\langle\uparrow| - |\downarrow\rangle\langle\downarrow|$, $\sigma_+ = |\uparrow\rangle\langle\downarrow|$, and $\sigma_- = \sigma_+^\dagger$; $a^\dagger$ and a are bosonic raising and lowering operators for the cavity; ω_q is the qubit excitation energy; ω_c is the resonator frequency; and g is the qubit-cavity coupling strength. Our focus will be on the QFI with respect to measurement of the coupling constant, g, i.e., $\theta = g$ in Eq. (2). Since we are concerned only with estimating the coupling, we work on resonance and in a rotating frame, or equivalently set $\omega_q = \omega_c = 0$. The state of the quantum probe undergoes open evolution described by the Gorini-Kossakowski-Sudarshan-Lindblad (GKSL) equation [55–58],

$$\dot{\rho} = -i[H, \rho] + \kappa\mathcal{D}[a](\rho) + \gamma\sum_{j=1}^N \mathcal{D}[\sigma_-^{(j)}](\rho), \tag{4}$$

where κ and γ are, respectively, resonator and qubit decay rates, and the dissipator

$$\mathcal{D}[\mathcal{O}](\rho) = \mathcal{O}\rho\mathcal{O}^\dagger - \tfrac{1}{2}(\mathcal{O}^\dagger\mathcal{O}\rho + \rho\mathcal{O}^\dagger\mathcal{O}). \tag{5}$$

With the system as described, the dynamics can be expressed in terms of the dimensionless time tg, decay rates κ/g and γ/g, and QFI (with respect to parameter g) can be represented as the dimensionless product $F(g)g^2$.

In principle, if the cavity excitation number is bounded above by the qubit number N, the Hilbert space of the combined qubit-cavity system has dimension $(N+1)2^N$. Operators on this Hilbert space (such as ρ), in turn, have $O(N^2 4^N)$ degrees of freedom, which severely limits computational capability even for moderately large N. However, spin-permutation symmetry—namely, the invariance of ρ under arbitrary permutations of its spins—reduces the degrees of freedom for a mixed state of N spins to a modest $O(N^3)$ [26,59–66], allowing us to perform calculations in a symmetric basis for the combined spin-boson system that grows as $O(N^5)$. Though individual terms on the right-hand side of Eq. (4) may break permutational symmetry, the sum of these terms does not. If ρ is initially invariant under all permutations of spins, therefore, this symmetry is preserved at

all times. This symmetry allows us to expand ρ in a basis of matrix elements of the form $|J,n\rangle\langle J,m|\otimes|\ell\rangle\langle k|$, where $J\in\{\frac{N}{2},\frac{N}{2}-1,\ldots,\frac{N \bmod 2}{2}\}$ is a total spin length, $n,m\in\{J,J-1,\ldots,-J\}$ are spin projections onto the spin quantization axis, and $\ell,k\in\{0,1,\ldots,N\}$ are cavity occupation numbers. Though the spin quantum numbers J and m are generally insufficient to uniquely determine the state of N spins when $J<N/2$, the values of additional quantum numbers are fixed by the requirement of spin-permutation symmetry [26]. We provide additional details about our numerical simulations (benchmarked in small-scale systems against QuTiP [67,68]) in Appendix A, and make our codes publicly available at Ref. [69].

Our main focus is on the case where the quantum probe is initialized in Dicke states of the qubits with resonator in its ground state,

$$|\text{D-}n\rangle=|\phi_n\rangle\otimes|0\rangle,\quad |\phi_n\rangle\propto S_+^n|0\rangle^{\otimes N}. \tag{6}$$

Here ϕ_n is a normalized Dicke state of N qubits, which can be equivalently defined as a uniform superposition of all N-qubit states with exactly n excitations, e.g.,

$$|\phi_1\rangle=\frac{1}{\sqrt{N}}(|100\cdots\rangle+|010\cdots\rangle+|001\cdots\rangle). \tag{7}$$

$|\phi_1\rangle$ is also known as the N-qubit W state [70]. For ease of language, we generally refer to D-n as the Dicke-n state of the qubit-resonator system.

For comparison with the D-n state we also consider the X-polarized state

$$|X\rangle=\left(\frac{|0\rangle+|1\rangle}{\sqrt{2}}\right)^{\otimes N}\otimes|0\rangle=\sum_m c_{Nm}\left|\frac{N}{2},m\right\rangle\otimes|0\rangle, \tag{8}$$

where $c_{Nm}=\sqrt{\binom{N}{N+m}/2^N}$, and the GHZ state

$$\begin{aligned}|\text{GHZ}\rangle&=\frac{1}{\sqrt{2}}(|0\rangle^{\otimes N}+|1\rangle^{\otimes N})\otimes|0\rangle\\&=\frac{1}{\sqrt{2}}\left(\left|\frac{N}{2},\frac{N}{2}\right\rangle+\left|\frac{N}{2},-\frac{N}{2}\right\rangle\right)\otimes|0\rangle,\end{aligned} \tag{9}$$

where we provide these states in the collective J,m spin basis, and both states are defined with the resonator in its ground state.

III. TIME DEPENDENCE OF THE QFI FOR N QUBITS

In Fig. 1 we show a plot of the time-dependent QFI for the Dicke-1 initial state for different values of N, keeping the decay constants on all the qubits and the resonators fixed. One sees that on average the QFI rises and then falls in time, with some oscillatory substructure superimposed. The region of largest QFI values and also the associated overall maximum QFI value increase in magnitude with increasing N. This behavior is not limited to the Dicke-1 state and happens for all the other Dicke-n states and for the GHZ and X-polarized initial states as well (see Appendix B for examples).

In Fig. 2 we provide plots of how the maximum QFI value scales with N. Note that we use N to quantify the resources

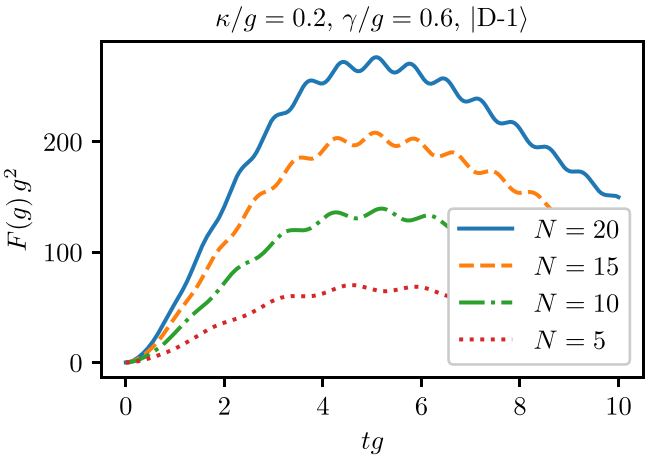

FIG. 1. QFI with respect to g as a function of time for different qubit numbers, N, for an initial Dicke-1 state with relatively small qubit (γ) and resonator (κ) decay rates. The peak structures increase with N for this case. Note that we display the QFI and time as the unitless quantities, $F(g)g^2$ and gt, respectively.

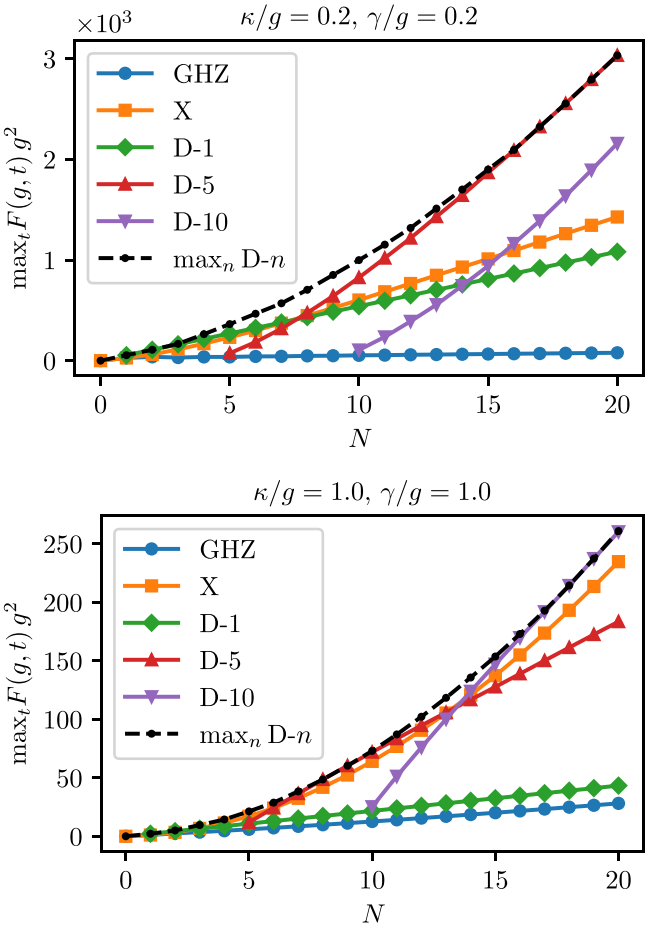

FIG. 2. Scaling of the maximum QFI with respect to time for fixed qubit and resonator decay rates, and different initial states. The upper and lower panels correspond to small and large values of the decay rates, respectively. The upper panel with $\kappa,\ \gamma\ll g$, corresponds to strong coupling between the qubits and the cavity, while the lower panel with $\kappa,\ \gamma\sim g$ corresponds to moderate coupling. Dashed black line shows, for each qubit number N, the time-optimized QFI maximized over choice of initial Dicke state.

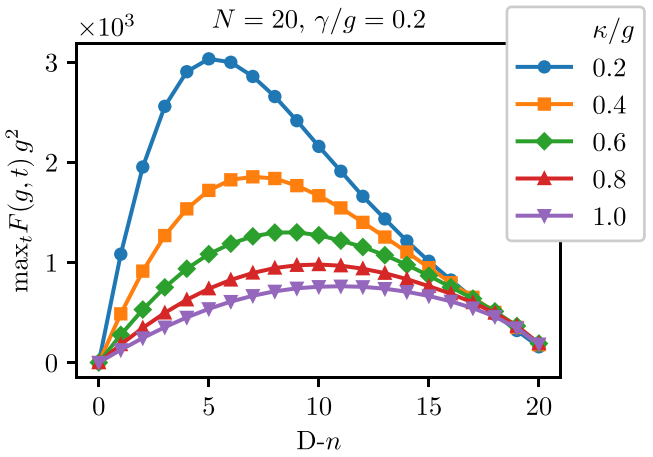

FIG. 3. Time-optimized mean QFI generation rate as a function of the initial Dicke excitation number for $N = 20$ qubits and different resonator decay rates, κ, for fixed qubit decay rate, γ.

that go into the measurement of g even though, strictly speaking, we have N qubits plus a resonator whose Hilbert space dimension grows as $N + 1$. It is interesting to note in Fig. 2 that the GHZ state, despite being maximally entangled by some measures, scales very poorly for both small and large values of decay rates. This is due to the fragility of the GHZ state to decoherence. For example, measuring just one qubit collapses the GHZ state into a separable state, whereas this is not the case for the W state or, indeed, most of the Dicke states. Of course this possible limitation of the GHZ state for quantum sensing has been noted many times, which has been motivation of exploration of other entangled states, not just Dicke states, such as graph states [15] and also motivation for the development of schemes to mitigate the effects of noise, e.g., Refs. [8,9,20,22].

For large values of the decay constants (lower panel of Fig. 2) the initially unentangled X-state scales in a manner almost comparable to the large excitation Dicke state. It is worth noting that the SQL, which applies to statistically independent probes, does not truly apply to this initial state because the spins interact with a shared resonator. We note, however, that the X state is competitive only with the best Dicke states in the limit of relatively high dissipation and low QFI magnitudes, i.e., in a limit less well suited to achieving high-precision sensing. For a metrology performance comparison between separable states like the X state and maximally entangled states see Ref. [71].

A. Optimal excitation number of Dicke states

Figure 2 shows that, depending on the number of qubits, N, there can be optimal Dicke state excitation numbers. In the case of low dissipation (upper panel of Fig. 2) for example, Dicke-1 has the larger QFI for $N = 5$–10, whereas Dicke-5 has the higher QFI for for $N > 10$. In Fig. 3 we plot the maximum value of the QFI against different Dicke excitation numbers for $N = 20$ and see that there is indeed an optimal value of the excitation number for which the maximum value of the QFI is the largest for each κ considered. By the geometric entanglement measure, for fixed N, it turns out that the most entangled Dicke state is equal to or close to Dicke-$N/2$ [72]. For the $N = 20$ case of Fig. 3, this would correspond to Dicke-10. The results of Fig. 3, however, show optimum Dicke states ranging from Dicke-5 at the lowest κ considered to Dicke-11 at the highest κ considered, again consistent with entanglement alone not being the best gauge of sensing quality and that a competition between degree of entanglement and resilience to noise leads to the optimum initial probe state.

Note that by focusing on measurements at times the maximum of $F(g,t)$ we are not explicitly considering the total measurement time as a resource to be minimized. If the times associated with individual shots are constant or not a significant resource, e.g., if state preparations, measurements, or other fixed experimental times dominate over actual system evolution times, then this is valid. Indeed, in previous work some of us showed that an experimental protocol can be developed using our optimum time idea that significantly reduces the total number of shots required to achieve a given precision in a parameter [23]. However, if the total measurement time associated with all the shots is considered a resource, and if for simplicity one neglects state preparation and other experimental factors, then one must consider $F(g,t)/t$ as the figure of merit to be maximized with respect to t [20] (see also Ref. [19], which minimized an associated uncertainty with measurement time in mind). Another scenario in which the total time is relevant is when the measured parameter is also time dependent, and there is a small window of time within which the value of the parameter has to be estimated. However, in our case, the coupling g that we are estimating is constant in time, and such considerations do not apply. For completeness, we have also carried out a number of calculations using maxima associated with $F(g,t)/t$ (see Appendix C) and have found very similar results to those described here.

Finally, we consider if certain ranges of the decay constants associated with the qubits and the resonator can lead to scaling that surpasses the standard quantum limit or SQL. To accomplish this, we fit $y(N) = aN^b + c$ to the maximum QFI vs N plots for a large range of decay constant values and extract the scaling exponent, b. The results of our numerical simulations are summarized in Fig. 4, where we plot the exponent b for different values of the decay constants for three different initial states: the X state, the Dicke-5, and Dicke-10. In these plots $b = 1$ corresponds to the SQL and $b = 2$ corresponds to the Heisenberg limit. Regarding the initially unentangled X state, scaling closer to the SQL limit occurs for low-decay constant values, as might be expected. A transition to much better than SQL scaling occurs for higher decay constants, possibly due to dissipation induced entanglement. However, as previously noted, the actual magnitudes of the QFI can be orders of magnitude smaller than what is achievable with Dicke states. For the Dicke states, it can be clearly seen that for certain low but finite values of the decay rates the Dicke states are able to go above the SQL and even achieve the Heisenberg limit.

In some previous work on noisy quantum metrology, [15,39,73–79] the importance of finding probe states that are resilient to noise rather than just highly entangled was pointed out, but the use of the optimal time for sensing was

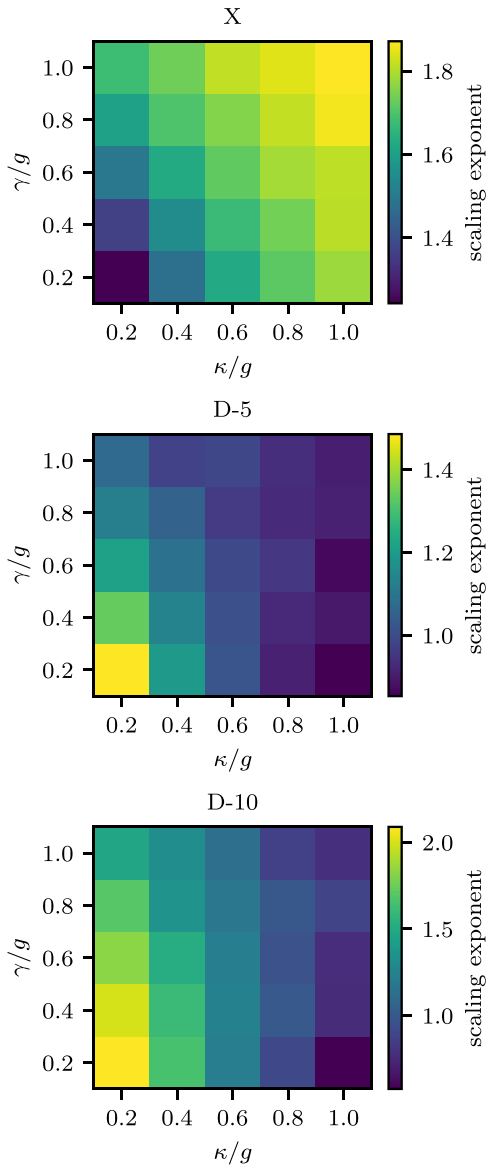

FIG. 4. The scaling exponent b obtained by fitting the time-maximized QFI to the qubit number N as $\max_t \mathrm{QFI}(t, N) = aN^b + c$ for different resonator and qubit decay rates κ and γ and three initial states. We see that when the qubits are strongly coupled to the cavity (relative to the losses), the Dicke states perform very well in terms of the scaling of the QFI with N while the initially unentangled X state performs better in the moderate coupling regime.

not considered. The use of optimum time ideas can be found in Refs. [20–22], but for much simpler model systems and different noise models than ours. Reference [20] was able to show Heisenberg limit scaling with GHZ states could be achieved for their system and noise model. References [21,22] also made use of Dicke states, but neither of these references was able to go beyond the SQL by making use of optimum time. Reference [22] was able to achieve HL in a steady-state limit where the collective phase noise considered in the model does not change the state and with auxiliary qubits via differential interferometry. Furthermore, earlier work suggests that separable probe states can never go beyond the SQL scaling. However, in our work we have demonstrated that for some models the subsequent dynamics allows the separable probe states to go beyond the SQL scaling and even achieve the Heisenberg limited scaling when the strategy of optimising the measurement time is also employed. In Ref. [22] it was pointed out that in the presence of correlated phases noise, X states can perform better than entangled ones. However, the scaling of the measurement uncertainty with N when the optimal time is always used was not considered.

It should be noted that the Dicke state HL limit results in Fig. 4 correspond to parameters in the strong coupling limit of $g \gg \kappa, \gamma$, which can sometimes be hard to achieve in practice. Interestingly the X-state results show near-HL limit scaling in a somewhat weaker or moderate coupling regime of $g \approx \kappa, \gamma$.

IV. CONCLUSIONS AND FUTURE DIRECTIONS

Many studies in noisy quantum metrology focus on uncoupled or weakly coupled systems of qubits. In contrast we study here systems of qubits coupled to a bosonic resonator (which in turn mediates qubit couplings). The dynamics of such systems, after preparation of some initial state, can be nontrivial and put to metrological advantage. We map out the behavior of such systems over a range of loss parameters for the qubits and the resonator, identifying optimal initial states and parameter ranges for going beyond the SQL. Among our interesting results include the use of Dicke states optimized with respect to excitation number and even the observation that initially separable states can yield scaling beyond the SQL under certain conditions. In coming to these conclusions we have made use of previously developed concepts in noisy quantum metrology, including the concept of optimal measurement times [19–23] and the general notion that some entangled states such as Dicke states can be more robust to noise [15,21,22].

For future work we will like to extend our study to include other noise models such as dephasing. Implementing our proposal to surpass the standard quantum limit in a laboratory can be a fruitful direction of research as well. The ability to produce Dicke states in the laboratory [27–37] offers the prospect of studying our proposal experimentally in a laboratory.

ACKNOWLEDGMENTS

We acknowledge very helpful discussions with A. Zang, T. Zhong, and Q. Langfitt for assistance with the calculations. This material is based upon work supported by the U.S. Department of Energy Office of Science National Quantum Information Science Research Centers. S.K.G. and Z.H.S. were supported by the Q-NEXT Center. Work performed at the Center for Nanoscale Materials, a U.S. Department of Energy Office of Science User Facility, was supported by the U.S. DOE Office of Basic Energy Sciences, under Contract No. DE-AC02-06CH11357. A.S. was supported by QuEST Grant No. Q-113 of the Department of Science and Technology, Government of India. The results in this work were obtained from simulations using ∼1000 CPU hours on the Bebop computing cluster at Argonne National Laboratory.

APPENDIX A: NUMERICAL SIMULATION DETAILS

Here we provide additional details about the numerical simulations of a spin-boson system performed for the main text. The codes for these simulations are available at Ref. [69].

For a system of N spins, we limit the boson excitation number to N. Spin-permutation symmetry then allows us to expand the density matrix in the form [26,59]

$$\rho = \sum_{J,n,m,\ell,k} \rho_{Jnm\ell k} |J,n\rangle\langle J,m| \otimes |\ell\rangle\langle k|, \tag{A1}$$

where $J \in \{\frac{N}{2}, \frac{N}{2}-1, \cdots\}$ is a (nonnegative) total spin length, $n, m \in \{J, J-1, \ldots, -J\}$ are spin projections onto the spin quantization axis, and $\ell, k \in \{0, 1, \ldots, N\}$ are boson excitation numbers.

The naive numerical representation of ρ in Eq. (A1) is with a five-dimensional array, with dimensions $(\lceil N/2 \rceil, \lceil N/2 \rceil, \lceil N/2 \rceil, N+1, N+1)$. However, about two-thirds of the elements in this array (namely, the elements with $|n|, |m| > J$) are guaranteed to be zero. In practice, we therefore combine (J, n, m) into a single integer index i, and flatten the density matrix into the three-dimensional array

$$|\rho) = \sum_{i,\ell,k} \rho_{i\ell k} |i,\ell,k\rangle. \tag{A2}$$

Operators acting ρ are then split into "left-acting" and "right-acting" variants to infer their action on $|\rho)$. The left- and right-acting boson ladder operators, for example, act on ρ as

$$a\rho \coloneqq a_L|\rho) = \sum_{i,\ell,k} \rho_{i\ell k} \sqrt{\ell} |i,\ell-1,k\rangle, \tag{A3}$$

$$\rho a^\dagger \coloneqq a_R^\dagger|\rho) = \sum_{i,\ell,k} \rho_{i\ell k} \sqrt{k} |i,\ell,k-1\rangle, \tag{A4}$$

which implies that $a_L = \mathbb{1} \otimes a \otimes \mathbb{1}$ and $a_R^\dagger = \mathbb{1} \otimes \mathbb{1} \otimes a$,

$$a_L = \mathbb{1} \otimes a \otimes \mathbb{1}, \quad a_R^\dagger = \mathbb{1} \otimes \mathbb{1} \otimes a, \tag{A5}$$

where $\mathbb{1}$ is the identity operator, and by slight abuse of notation the annihilation operators a on the right-hand side of Eq. (A5) act on the Hilbert space of the boson alone [whereas the operators a on the left-hand side of Eqs. (A3) and (A4) act on the joint spin-boson Hilbert space].

Left- and right-acting collective spin operators act on the first tensor factor of $|\rho)$ and can be constructed from

$$S_z = \sum_{J,m} m |J,m\rangle\langle J,m|, \tag{A6}$$

$$S_\pm = \sum_{J,m} \sqrt{J(J+1) - m(m\pm1)} |J,m\pm1\rangle\langle J,m|, \tag{A7}$$

where the sums implicitly restrict $|m| \leqslant J$, and the left- and right-acting variants of S_z, $S_\pm$ on $|\rho)$ can be constructed using the same index mapping used to map $|J,n\rangle\langle J,m| \to i$ for $\rho \to |\rho)$.

The final ingredient necessary to simulate the results in the main text is the evaluation of dissipation terms of the form

$$\mathcal{L}[s] = \sum_{j=1}^{N} \mathcal{D}[s^{(j)}](\rho), \tag{A8}$$

where $s = s_{\mathbb{1}} + s_+\sigma_+ + s_-\sigma_- + s_z\sigma_z$ is a single-qubit operator defined in terms of the Pauli matrices σ_α. The effect of these dissipation terms in the (J, n, m) basis were worked out in Ref. [59], and specifically in Eqs. (39)–(46) therein.

In the special case that $s = \sigma_-$, the relevant results in Ref. [59] reduce to

$$\mathcal{L}[s] = \sum_{j=1}^{N} \sigma_-^{(j)} \rho \sigma_+^{(j)} - \frac{1}{4}(S_z\rho + \rho S_z), \tag{A9}$$

where

$$\begin{aligned}
&\sum_{j=1}^{N} \sigma_-^{(j)} |J,n\rangle\langle J,m| \sigma_+^{(j)} \\
&\quad = \frac{1}{2J}\left(1 + \frac{\alpha_N^{J+1}}{d_N^J}\frac{2J+1}{J+1}\right) A_-^{J\ell} |J,\ell-1\rangle\langle J,k-1| A_-^{Jk} \\
&\qquad + \frac{\alpha_N^J}{2Jd_N^J} B_-^{J\ell} |J-1,\ell-1\rangle\langle J-1,k-1| B_-^{Jk} \\
&\qquad + \frac{\alpha_N^{J+1}}{2(J+1)d_N^J} D_-^{J\ell} |J+1,\ell-1\rangle\langle J+1,k-1| D_-^{Jk},
\end{aligned} \tag{A10}$$

where

$$\alpha_N^J = \binom{N}{N/2-J}, \tag{A11}$$

$$d_N^J = \binom{N}{N/2-J} \times \frac{2J+1}{N/2+J+1}, \tag{A12}$$

$$A_-^{J\ell} = \sqrt{(J+\ell)(J-\ell+1)}, \tag{A13}$$

$$B_-^{J\ell} = -\sqrt{(J+\ell)(J+\ell-1)}, \tag{A14}$$

$$D_-^{J\ell} = \sqrt{(J-\ell+1)(J-\ell+2)}. \tag{A15}$$

These ingredients are sufficient to determine the state ρ at all times by numerically integrating the equations of motion in Eq. (4). We perform this numerical integration using the `DOP853` method of `scipy.integrate.solve_ivp` [80], with relative and absolute error tolerances of $\epsilon_{\text{rtol}} = \epsilon_{\text{atol}} = 10^{-10}$. We benchmark the correctness and accuracy of our methods against small-scale ($N \leqslant 5$) simulations performed with the Quantum Toolbox in Python QuTiP [67,68].

Denoting the state ρ at time t after evolving under the equations of motion in Eq. (4) with coupling constant g as $\rho(g,t)$, the QFI of ρ with respect to g at time t is then determined by evaluating Eq. (2) using finite differences, namely,

$$F(g,t) = 2\sum_{a,b} \frac{|\langle\lambda_a|\partial_g\rho(g,t)|\lambda_b\rangle^2|}{\lambda_a + \lambda_b}, \tag{A16}$$

where the sum is taken over values of a, b for which $\lambda_a + \lambda_b \neq 0$, and

$$\partial_g\rho(g,t) \approx \frac{\rho(g+\delta g/2,t) - \rho(g-\delta g/2,t)}{\delta g} \tag{A17}$$

with a positive $\delta \ll 1$. We set $\delta = 10^{-3}$ in our simulations, which are performed in units with $g = 1$ for improved numerical stability.

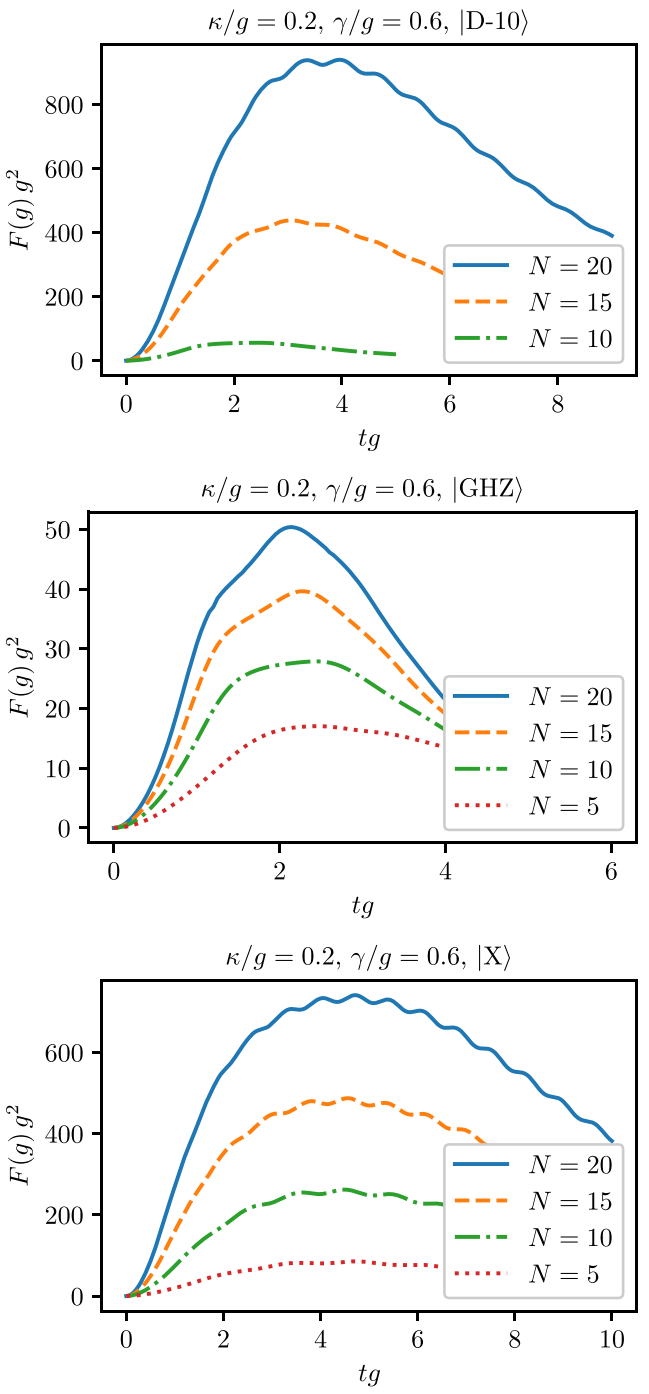

FIG. 5. Time dependence of QFI for different probe states. Each of the figures shows how the maximum value of the QFI changes with time and also with varying N.

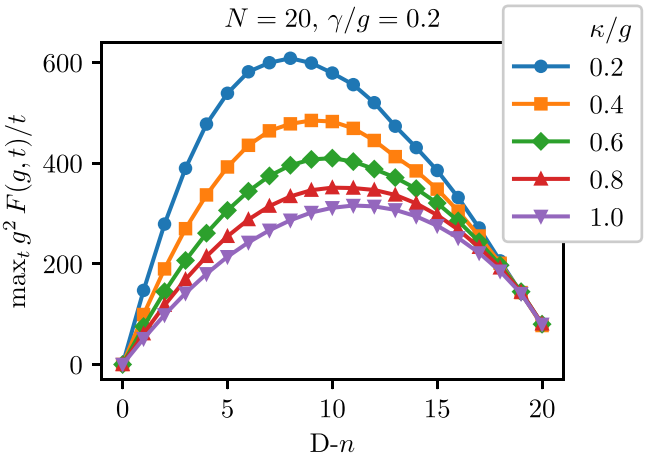

FIG. 6. Variation of the maximum QFI$(t)/t$ (with respect to time) with Dicke excitation number for $N = 20$ qubits and varying resonator decay rate, κ, for fixed qubit decay rate, γ.

The structure of the equations of motion, Eq. (4), and Hamiltonian, Eq. (3), lead to useful scalings. For simplicity, consider the rotating frame limit that we use in the main text, $\omega_q = \omega_c = 0$. One can easily see that if one expresses the equations of motion in terms of a dimensionless time, $\tilde{t} = gt$, then $d\rho/d\tilde{t}$ involves the dissipator parameters divided by g, i.e., $\tilde{\kappa} = \kappa/g$, $\tilde{\gamma} = \gamma/g$ and the qubit-cavity Hamiltonian coupling becomes $\tilde{g} = 1$. Thus, calculations with $\tilde{g} = 1$ can yield information about results for all g if one reinterprets the dissipator parameters as being divided by g. It is also easy to show that the QFI for a particular value of g, $F(g)$, can be related to the QFI calculated with respect to $\tilde{g}$ at $\tilde{g} = 1$, $F(\tilde{g})|_{\tilde{g}=1}$ by: $F(g)\,g^2 = F(\tilde{g})|_{\tilde{g}=1}$.

A final subtlety of our simulations is the treatment of floating-point errors, which can result in numerical instabilities of $F(g,t)$ due to the denominator $\lambda_a + \lambda_b$ in Eq. (A16). Specifically, floating-point errors cause negative eigenvalues of ρ to pick up a small nonzero value. To mitigate instabilities from small nonzero eigenvalues in the denominator of

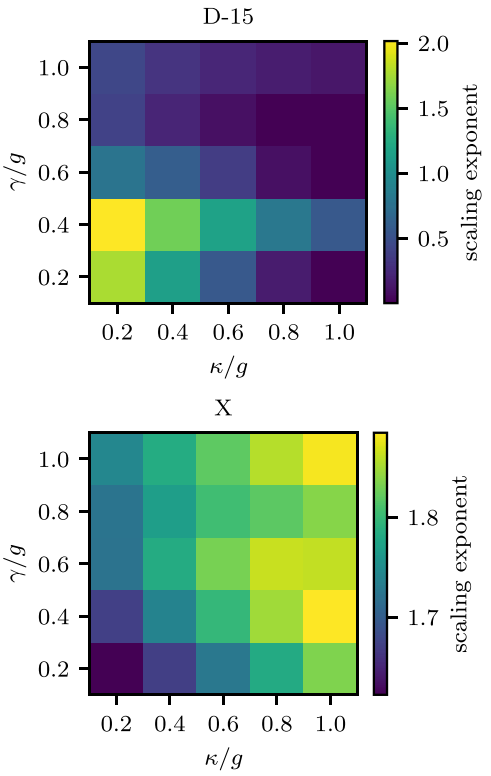

FIG. 7. Scaling exponents b from a three-parameter fit to $\max_t \text{QFI}(t,N)/t \sim aN^b + c$, where N is the qubit number, for the Dicke-15 state and the polarized-X state.

Eq. (A16), we identify $\epsilon_{\text{err}} = |\min_a \lambda_a|$ as the scale of floating-point errors in ρ. We note that $\min_a \lambda_a$ is always negative in practice, since floating-point errors cause each zero eigenvalue of ρ to become negative with ∼50% probability. When evaluating $F(g,t)$, we then set eigenvalues less than $10\epsilon_{\text{err}}$ to 0, and sum over all values of a, b for which $\lambda_a + \lambda_b > 10^{-8}$.

APPENDIX B: TIME DEPENDENCE OF QFI FOR VARYING SYSTEM SIZE AND PROBE STATES

Here we provide a few more examples of how the optimal time for performing measurements on the quantum system changes as we change the number of qubits and the probe states. It can be clearly seen in Fig. 5 that for different initial states the optimal time for performing the measurement changes as we change the number of qubits.

APPENDIX C: COMPUTATIONS WITH TIME AS A RESOURCE

Let T be the total time the experimenter has and the t be the measurement time. Then the total number of applications of the quantum probe is $M = T/t$. The Cramér-Rao bound can now be rephrased as

$$\delta\hat{\theta}^2 \geqslant \frac{1}{TF(\theta)/t}. \tag{C1}$$

The quantity that we optimize with respect to time then becomes the $F(t,\theta)/t$ instead of just F. Our results are provided in the Figs. 6 and 7.

Figure 6 shows the time-optimized average QFI generation rate $\max_t F(g,t)/t$ as a function of the initial Dicke excitation number for different resonator decay rates κ. We see that the behavior of $\max_t F(g,t)/t$ mirrors that of the time-optimized QFI $\max_t F(g,t)$ in Fig. 3, indicating that our conclusions regarding the optimal excitation number for Dicke states still holds if we consider time as a resource. The same is true for the scaling of the QFI at optimal times as a function of N as well, in Fig. 7. Our main conclusions therefore remain unchanged if we treat the total time T as a resource.

[1] V. Giovannetti, S. Lloyd, and L. Maccone, Advances in quantum metrology, Nature Photon **5**, 222 (2011).

[2] G. Tóth and I. Apellaniz, Quantum metrology from a quantum information science perspective, J. Phys. A: Math. Theor. **47**, 424006 (2014).

[3] W. Nawrocki, *Introduction to Quantum Metrology*, 2nd ed. (Springer Nature, Cham, Switzerland, 2019).

[4] E. Polino, M. Valeri, N. Spagnolo, and F. Sciarrino, Photonic quantum metrology, AVS Quantum Sci. **2**, 024703 (2020).

[5] V. Giovannetti, S. Lloyd, and L. Maccone, Quantum-enhanced measurements: Beating the standard quantum limit, Science **306**, 1330 (2004).

[6] L. Pezzé and A. Smerzi, Mach-Zehnder interferometry at the Heisenberg limit with coherent and squeezed-vacuum light, Phys. Rev. Lett. **100**, 073601 (2008).

[7] M. B. Plenio and S. F. Huelga, Sensing in the presence of an observed environment, Phys. Rev. A **93**, 032123 (2016).

[8] R. Demkowicz-Dobrzanski, J. Czajkowski, and P. Sekatski, Adaptive quantum metrology under general Markovian noise, Phys. Rev. X **7**, 041009 (2017).

[9] S. Zhou, M. Zhang, J. Preskill, and L. Jiang, Achieving the Heisenberg limit in quantum metrology using quantum error correction, Nat. Commun. **9**, 78 (2018).

[10] W. Dür, M. Skotiniotis, F. Fröwis, and B. Kraus, Improved quantum metrology using quantum error correction, Phys. Rev. Lett. **112**, 080801 (2014).

[11] Z. Huang, G. K. Brennen, and Y. Ouyang, Imaging stars with quantum error correction, Phys. Rev. Lett. **129**, 210502 (2022).

[12] E. M. Kessler, I. Lovchinsky, A. O. Sushkov, and M. D. Lukin, Quantum error correction for metrology, Phys. Rev. Lett. **112**, 150802 (2014).

[13] D. Layden, S. Zhou, P. Cappellaro, and L. Jiang, Ancilla-free quantum error correction codes for quantum metrology, Phys. Rev. Lett. **122**, 040502 (2019).

[14] N. Shettell, W. J. Munro, D. Markham, and K. Nemoto, Practical limits of error correction for quantum metrology, New J. Phys. **23**, 043038 (2021).

[15] N. Shettell and D. Markham, Graph states as a resource for quantum metrology, Phys. Rev. Lett. **124**, 110502 (2020).

[16] Y. Matsuzaki, S. C. Benjamin, and J. Fitzsimons, Magnetic field sensing beyond the standard quantum limit under the effect of decoherence, Phys. Rev. A **84**, 012103 (2011).

[17] A. W. Chin, S. F. Huelga, and M. B. Plenio, Quantum metrology in non-Markovian environments, Phys. Rev. Lett. **109**, 233601 (2012).

[18] A. Altherr and Y. Yang, Quantum metrology for non-Markovian processes, Phys. Rev. Lett. **127**, 060501 (2021).

[19] S. F. Huelga, C. Macchiavello, T. Pellizzari, A. K. Ekert, M. B. Plenio, and J. I. Cirac, Improvement of frequency standards with quantum entanglement, Phys. Rev. Lett. **79**, 3865 (1997).

[20] R. Chaves, J. B. Brask, M. Markiewicz, J. Kolodynski, and A. Acin, Noisy metrology beyond the standard quantum limit, Phys. Rev. Lett. **111**, 120401 (2013).

[21] F. Fröwis, M. Skotinotis, B. Kraus, and W. Dür, Optimal quantum states for frequency estimation, J. Phys. **16**, 083010 (2014).

[22] S. Altenburg, S. Wolk, G. Toth, and O. Guhne, Optimized parameter estimation in the presence of collective phase noise, Phys. Rev. A **94**, 052306 (2016).

[23] Z. H. Saleem, A. Shaji, and S. K. Gray, Optimal time for sensing in open quantum systems, Phys. Rev. A **108**, 022413 (2023).

[24] H. Cramér, A contribution to the theory of statistical estimation, Scand. Actuarial J. **1946**, 85 (1946).

[25] R. H. Dicke, Coherence in spontaneous radiation processes, Phys. Rev. **93**, 99 (1954).

[26] N. Shammah, S. Ahmed, N. Lambert, S. De Liberato, and F. Nori, Open quantum systems with local and collective incoherent processes: Efficient numerical simulations using permutational invariance, Phys. Rev. A **98**, 063815 (2018).

[27] Y.-Q. Zou, L.-N. Wu, Q. Liu, X.-Y. Luo, S.-F. Guo, J.-H. Cao, M. K. Tey, and L. You, Beating the classical precision limit with spin-1 Dicke states of more than 10,000 atoms, Proc. Natl. Acad. Sci. USA **115**, 6381 (2018).

[28] L. Chen, L. Lu, L. Xia, Y. Lu, S. Zhu, and X.-S. Ma, On-chip generation and collectively coherent control of the superposition of the whole family of Dicke states, Phys. Rev. Lett. **130**, 223601 (2023).

[29] A. Chiuri, G. Vallone, N. Bruno, C. Macchiavello, D. Bruß, and P. Mataloni, Hyperentangled mixed phased Dicke states: Optical design and detection, Phys. Rev. Lett. **105**, 250501 (2010).

[30] F. Haas, J. Volz, R. Gehr, J. Reichel, and J. Estève, Entangled states of more than 40 atoms in an optical fiber cavity, Science **344**, 180 (2014).

[31] H. Häffner, W. Hänsel, C. F. Roos, J. Benhelm, D. Chek-al-kar, M. Chwalla, T. Körber, U. D. Rapol, M. Riebe, P. O. Schmidt *et al.*, Scalable multiparticle entanglement of trapped ions, Nature (London) **438**, 643 (2005).

[32] D. B. Hume, C. W. Chou, T. Rosenband, and D. J. Wineland, Preparation of Dicke states in an ion chain, Phys. Rev. A **80**, 052302 (2009).

[33] A. Noguchi, K. Toyoda, and S. Urabe, Generation of Dicke states with phonon-mediated multilevel stimulated Raman adiabatic passage, Phys. Rev. Lett. **109**, 260502 (2012).

[34] R. Prevedel, G. Cronenberg, M. S. Tame, M. Paternostro, P. Walther, M. S. Kim, and A. Zeilinger, Experimental realization of Dicke states of up to six qubits for multiparty quantum networking, Phys. Rev. Lett. **103**, 020503 (2009).

[35] K. Toyoda, T. Watanabe, T. Kimura, S. Nomura, S. Haze, and S. Urabe, Generation of Dicke states using adiabatic passage, Phys. Rev. A **83**, 022315 (2011).

[36] W. Wieczorek, R. Krischek, N. Kiesel, P. Michelberger, G. Tóth, and H. Weinfurter, Experimental entanglement of a six-photon symmetric Dicke state, Phys. Rev. Lett. **103**, 020504 (2009).

[37] S. Yu, M. Titze, Y. Zhu, X. Liu, and H. Li, Observation of scalable and deterministic multi-atom Dicke states in an atomic vapor, Opt. Lett. **44**, 2795 (2019).

[38] V. Paulisch, M. Perarnau-Llobet, A. González-Tudela, and J. I. Cirac, Quantum metrology with one-dimensional superradiant photonic states, Phys. Rev. A **99**, 043807 (2019).

[39] Z. Zhang and L. M. Duan, Quantum metrology with Dicke squeezed states, New J. Phys. **16**, 103037 (2014).

[40] L. Pezze, A. Smerzi, M. K. Oberthaler, R. Schmied, and P. Treutlein, Quantum metrology with nonclassical states of atomic ensembles, Rev. Mod. Phys. **90**, 035005 (2018).

[41] S. Aktar, A. Bärtschi, A.-H. A. Badawy, and S. Eidenbenz, A divide-and-conquer approach to Dicke state preparation, IEEE Trans. Quantum Eng. **3**, 1 (2022).

[42] K. Chakraborty, B.-S. Choi, A. Maitra, and S. Maitra, Efficient quantum algorithms to construct arbitrary Dicke states, Quantum Info. Proc. **13**, 2049 (2014).

[43] S. S. Ivanov, N. V. Vitanov, and N. V. Korolkova, Creation of arbitrary Dicke and NOON states of trapped-ion qubits by global addressing with composite pulses, New J. Phys. **15**, 023039 (2013).

[44] S. Kasture, Scalable approach to generation of large symmetric Dicke states, Phys. Rev. A **97**, 043862 (2018).

[45] L. Lamata, C. E. López, B. P. Lanyon, T. Bastin, J. C. Retamal, and E. Solano, Deterministic generation of arbitrary symmetric states and entanglement classes, Phys. Rev. A **87**, 032325 (2013).

[46] F. Mu, Y. Gao, H. Yin, and G. Wang, Dicke state generation via selective interactions in a Dicke-Stark model, Opt. Express **28**, 39574 (2020).

[47] S. Raghavan, H. Pu, P. Meystre, and N. P. Bigelow, Generation of arbitrary Dicke states in spinor Bose–Einstein condensates, Opt. Commun. **188**, 149 (2001).

[48] V. M. Stojanović and J. K. Nauth, Dicke-state preparation through global transverse control of Ising-coupled qubits, Phys. Rev. A **108**, 012608 (2023).

[49] Y. Wang and B. M. Terhal, Preparing Dicke states in a spin ensemble using phase estimation, Phys. Rev. A **104**, 032407 (2021).

[50] J.-H. Wei, B. Qi, H.-Y. Dai, J.-H. Huang, and M. Zhang, Deterministic generation of symmetric multi-qubit Dicke states: An application of quantum feedback control, IET Control Theory Appl. **9**, 2500 (2015).

[51] C. Wu, C. Guo, Y. Wang, G. Wang, X.-L. Feng, and J.-L. Chen, Generation of Dicke states in the ultrastrong-coupling regime of circuit QED systems, Phys. Rev. A **95**, 013845 (2017).

[52] C. Zhao and L. Ye, Efficient scheme for the preparation of symmetric Dicke states via cross-Kerr nonlinearity, Phys. Lett. A **375**, 401 (2011).

[53] A. S. Holevo, *Probabilistic and Statistical Aspects of Quantum Theory* (Springer Science & Business Media, New York, 2011), Vol. 1.

[54] J. Liu, H. Yuan, X.-M. Lu, and X. Wang, Quantum Fisher information matrix and multiparameter estimation, J. Phys. A: Math. Theor. **53**, 023001 (2019).

[55] V. Gorini, A. Kossakowski, and E. C. G. Sudarshan, Completely positive dynamical semigroups of *N*-level systems, J. Math. Phys. **17**, 821 (1976).

[56] G. Lindblad, On the generators of quantum dynamical semigroups, Commun. Math. Phys. **48**, 119 (1976).

[57] C. Dariusz and S. Pascazio, A brief history of the GKLS equation, Open Syst. Info. Dyn. **24**, 1740001 (2017).

[58] D. Manzano, A short introduction to the Lindblad master equation, AIP Adv. **10**, 025106 (2020).

[59] B. A. Chase and J. M. Geremia, Collective processes of an ensemble of spin-1/2 particles, Phys. Rev. A **78**, 052101 (2008).

[60] B. Q. Baragiola, B. A. Chase, and J. M. Geremia, Collective uncertainty in partially polarized and partially decohered spin-1/2 systems, Phys. Rev. A **81**, 032104 (2010).

[61] T. Moroder, P. Hyllus, G. Tóth, C. Schwemmer, A. Niggebaum, S. Gaile, O. Gühne, and H. Weinfurter, Permutationally invariant state reconstruction, New J. Phys. **14**, 105001 (2012).

[62] L. Novo, T. Moroder, and O. Gühne, Genuine multiparticle entanglement of permutationally invariant states, Phys. Rev. A **88**, 012305 (2013).

[63] M. Xu, D. A. Tieri, and M. J. Holland, Simulating open quantum systems by applying SU(4) to quantum master equations, Phys. Rev. A **87**, 062101 (2013).

[64] M. Bolaños and P. Barberis-Blostein, Algebraic solution of the Lindblad equation for a collection of multilevel systems coupled to independent environments, J. Phys. A: Math. Theor. **48**, 445301 (2015).

[65] N. Shammah, N. Lambert, F. Nori, and S. De Liberato, Superradiance with local phase-breaking effects, Phys. Rev. A **96**, 023863 (2017).

[66] Y. Zhang, Y.-X. Zhang, and K. Molmer, Monte-Carlo simulations of superradiant lasing, New J. Phys. **20**, 112001 (2018).

[67] J. R. Johansson, P. D. Nation, and F. Nori, QuTiP: An open-source python framework for the dynamics of open quantum systems, Comput. Phys. Commun. **183**, 1760 (2012).

[68] J. Johansson, P. Nation, and F. Nori, QuTiP 2: A python framework for the dynamics of open quantum systems, Comput. Phys. Commun. **184**, 1234 (2013).

[69] M. A. Perlin, spin-boson, https://github.com/perlinm/spin-boson (2023).

[70] W. Dür, G. Vidal, and J. I. Cirac, Three qubits can be entangled in two inequivalent ways, Phys. Rev. A **62**, 062314 (2000).

[71] M. Beau and A. del Campo, Nonlinear quantum metrology of many-body open systems, Phys. Rev. Lett. **119**, 010403 (2017).

[72] J. Martin, O. Giraud, P. A. Braun, D. Braun, and T. Bastin, Multiqubit symmetric states with high geometric entanglement, Phys. Rev. A **81**, 062347 (2010).

[73] S. Kurdziałek, W. Górecki, F. Albarelli, and R. Demkowicz-Dobrzański, Using adaptiveness and causal superpositions against noise in quantum metrology, Phys. Rev. Lett. **131**, 090801 (2023).

[74] Q. Liu, Z. Hu, H. Yuan, and Y. Yang, Optimal strategies of quantum metrology with a strict hierarchy, Phys. Rev. Lett. **130**, 070803 (2023).

[75] R. Nichols, T. R. Bromley, L. A. Correa, and G. Adesso, Practical quantum metrology in noisy environments, Phys. Rev. A **94**, 042101 (2016).

[76] M. Perarnau-Llobet, D. Malz, and J. I. Cirac, Weakly invasive metrology: Quantum advantage and physical implementations, Quantum **5**, 446 (2021).

[77] W. Wang, Z.-J. Chen, X. Liu, W. Cai, Y. Ma, X. Mu, X. Pan, Z. Hua, L. Hu, Y. Xu *et al.*, Quantum-enhanced radiometry via approximate quantum error correction, Nat. Commun. **13**, 3214 (2022).

[78] C. Zhang, T. R. Bromley, Y.-F. Huang, H. Cao, W.-M. Lv, B.-H. Liu, C.-F. Li, G.-C. Guo, M. Cianciaruso, and G. Adesso, Demonstrating quantum coherence and metrology that is resilient to transversal noise, Phys. Rev. Lett. **123**, 180504 (2019).

[79] S. Zhou, S. Michalakis, and T. Gefen, Optimal protocols for quantum metrology with noisy measurements, PRX Quantum **4**, 040305 (2023).

[80] P. Virtanen, R. Gommers, T. E. Oliphant, M. Haberland, T. Reddy, D. Cournapeau, E. Burovski, P. Peterson, W. Weckesser, J. Bright *et al.*, SciPy 1.0: Fundamental algorithms for scientific computing in python, Nat. Methods **17**, 261 (2020).